Decay Kinetics of Nanoscale Corrugation Gratings on Polymer Surface: Evidence for Polymer Flow below the Glass Temperature

Elke Buck,[†] Kirstin Petersen,[‡] Markus Hund,[§] Georg Krausch,[§] and Diethelm Johannsmann*,[†]

Institute of Physical Chemistry, Technical University Clausthal, Arnold-Sommerfeld-Str. 4, 38678 Clausthal-Zellerfeld, Germany; MPI for Polymer Research, Ackermannweg 10, 55128 Mainz, Germany; and Physikalische Chemie II and Bayreuther Zentrum für Kolloide und Grenzflächen (BZKG), Universität Bayreuth, 95440 Bayreuth, Germany

Received March 1, 2004; Revised Manuscript Received July 26, 2004

ABSTRACT: The near-surface rheology of polystyrene films at temperatures around T_g was probed via the decay kinetics of shallow, nanoscale surface corrugation gratings. The gratings were created via hot embossing with a stepped silicon template. The wavelengths are distributed in a range between 25 and 60 nm and have a modulation depth of about 0.8 nm peak-to-peak. Upon heating, one observes a surface tension-driven decay of the surface corrugation at temperatures more than 30 deg below the bulk T_g. Such a fast decay is unexpected and indicates a strongly lowered glass temperature near the surface.

Introduction

Adhesion and friction on polymer surfaces are to a large extent governed by the flow properties of the material close to the interface.[1,2] For example, the energy required to separate two soft polymer surfaces usually exceeds the thermodynamic free energy by orders of magnitude.[3] The excess debonding energy is spent on plastic deformation, often connected to the formation of filaments. A similar statement holds for sliding friction.[4] The dissipated energy is mostly spent on the deformation of small asperities across which the contact is made. Frictional resistance and wear strongly depend on the mechanical properties of the material close to the interface. In particular, they depend on whether the surface is glassy or soft.

As has been discussed in detail in the recent years, the glass temperature, T_g, of polymers can be affected by geometric confinement.[5] Free-standing films showed a decrease of T_g of up to 40 K.[6] Many of these experiments were carried out on thin films. Both from a fundamental perspective and from the viewpoint of application, it seems attractive to perform experiments on the surfaces of bulk polymers rather than on thin films. Kajiyama and co-workers have performed friction force microscopy on polymer surfaces at various temperatures around T_g.[1] They find a decreased near-surface T_g in most cases. However, in friction force microscopy the local stress exerted by the tip is often very high and may therefore cause stress-induced softening. Tsui and co-workers have followed a similar approach, but they base the analysis on adhesion hysteresis rather than sliding friction.[2] Shear force modulation is another option.[7] Forrest et al. have probed the embedding of small particles into the polymer surface. They decorated polystyrene films which had been spin-cast onto quartz crystal resonators with small glass beads.[8] When heating the sample to the glass transition, the bandwidth of the resonance decreases, which is explained by an embedding process. Faupel and co-workers have investigated a similar phenomenon by photoelectron spectroscopy on metal clusters deposited on polymer films.[9] The reorientation of polymer segments close to the interface has been probed by near-edge X-ray absorption fine structure (NEXAFS).[10] These authors did not find complete relaxation below T_g. Tolan and co-workers have used capillary waves monitored by X-ray reflectivity to probe the near-surface dynamics of glass-forming liquids.[11] The capillary waves on glycerol were found to freeze much above T_g. In related work employing specular and diffuse X-ray scattering on polystyrene films, they find that capillary wave calculations assuming van der Waals substrate−film interactions cannot satisfactorily explain the data.[12]

We report on surface-rheological experiments, where the polymer flow is given by the surface-tension-driven decay of imprinted surface corrugation gratings. By nature, this is a very gentle process. One can be sure to be in the regime where linear stress−strain relations hold. Kerle et al. have used atomic force microscopy to investigate the decay of surface roughness on the nanometer scale as a function of annealing time.[13] They find a partial annealing at $T < T_g$, on one hand, and an incomplete decay even for long annealing times at temperatures much above T_g, on the other. Li and co-workers have observed the decay of surface waves of thin films on patterned silicon gratings.[14] They found that the apparent diffusion coefficient was smaller than in the bulk. Johannsmann and co-workers have used the decay kinetics of shallow sinusoidal surface waves to probe the near-surface rheology of polystyrene (PS)[15] and poly(methyl methacrylate) (PMMA).[16] In these investigations the wavelength of the roughness was in the micron range. The master used for imprinting had been produced by photolithography, and the observation of the decay was done by optical diffraction. Shallow periodic structures are attractive for interface rheology because the flow field is known and a quantitative analysis is possible. It turns out that the penetration depth of the surface wave is equal to the wavelength of the corrugation grating divided by 2π. For a wavelength

[†] Technical University Clausthal.
[‡] MPI for Polymer Research.
[§] Universität Bayreuth.
* Corresponding author: phone +49 (0)-5323-72 3768; fax +49 (0)-5323-72 4835; e-mail johannsmann@pc.tu-clausthal.de.

10.1021/ma049595z CCC: $27.50 © 2004 American Chemical Society
Published on Web 10/19/2004

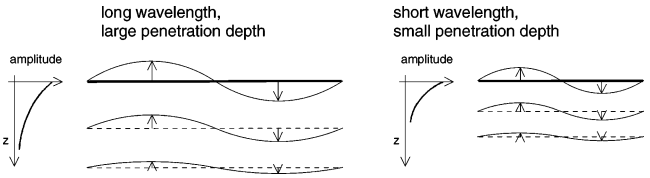

Figure 1. Decay pattern of surface waves on a highly viscous liquid. The penetration depth is equal to the wavelength divided by 2π.

of 600 nm, this amounts to a penetration depth of about 100 nm. When using optical gratings with a wavelength in the micron range, the technique is not very surface-sensitive since it probes a depth which is considerably larger than the characteristic length scales commonly encountered in polymers (such as the radius of gyration, R_g).

Here, we describe an extension of these measurements, where the lithographic master has been replaced by a nanoscopically corrugated silicon wafer[17,18] and the detection is performed using atomic force microscopy. The average wavelength of the master was 40 nm, which corresponds to a penetration depth of about 7 nm. In consequence, the surface sensitivity of the technique is considerably improved compared to earlier studies.

Theory

In the following we briefly outline a continuum description of the decay of shallow sinusoidal surface waves with wave vector q.[19,20] If the surface is not sinusoidally corrugated, the surface structure can be Fourier-decomposed. The analysis below then holds for the individual Fourier components. The medium is assumed to be homogeneous, isotropic, and incompressible with the complex shear modulus $G(\omega)$ entirely determining its rheology. Effects of gravity, external pressure, and inertia are neglected. We assume a linear stress−strain relationship. The flow field $\mathbf{v}(x,z)$ is governed by the continuity equation

$$\nabla\cdot\mathbf{v}(x,z) = 0 \tag{1}$$

and the Laplace equation

$$\nabla^2\mathbf{v}(x,z) = 0 \tag{2}$$

where x is the coordinate in the plane of the sample along the grating's wave vector and z is the coordinate normal to the surface. Since there is no flow along the third axis, this index ("y") was dropped. Equation 2 follows from the Navier−Stokes equation where all terms apart from the viscous drag $\eta\nabla^2\nu$ (η the viscosity) have been neglected. For the displacement pattern we make the ansatz

$$u_x(x,z,t) = -u_{x,0}(t)\sin(qx)\exp(\alpha z) \tag{3}$$

$$u_z(x,z,t) = u_{z,0}(t)\cos(qx)\exp(\alpha z) \tag{4}$$

where u is the displacement of a given volume element from its equilibrium position. The continuity equation implies that $u_{x,0}(t) = u_{z,0}(t) = u_0(t)$, where $u_0(t)$ is a prefactor depending on time. From the Laplace equation, we infer that $\alpha = q$. The penetration depth of the surface wave $\alpha^{-1} = q^{-1}$ is therefore equal to the lateral wavelength divided by 2π (Figure 1). The penetration depth quantifies the meaning of the term "near surface".

In the following, we calculate the decay rate $(\mathrm{d}u(t)/\mathrm{d}t)/u(t)$. The decay kinetics is governed by the balance between the vertical stress exerted by the corrugated surface, P_γ, and the stress caused by the gradients in the flow field, P_{zz}. The vertical stress from the surface is equal to the Laplace pressure. We have[19]

$$P_\gamma(x,t,z{=}0) = -\gamma u_0(t)q^2\cos(qx) \tag{5}$$

where γ is the surface tension $u_0(t)q^2\cos(qx)$ is the curvature of the surface. The viscous stress caused by gradients of the flow field is given by[19]

$$P_{zz} = 2\eta\frac{\partial v_z(x,t)}{\partial z} = 2\eta q\frac{\mathrm{d}u_0(t)}{\mathrm{d}t}\cos(qx) \tag{6}$$

Equating these two stresses, we arrive at

$$\frac{\mathrm{d}u_0(t)}{\mathrm{d}t} = -\frac{1}{2}\frac{q\gamma}{\eta}u_0(t) \tag{7}$$

This differential equation is solved by exponential decays of the form

$$u_0(t) = u_{0,0}\mathrm{e}^{-Rt} \tag{8}$$

where $u_{0,0}$ is the initial amplitude. The decay rate, R, is given by

$$R = \frac{q\gamma}{2\eta} \tag{9}$$

As expected, the decay rate is proportional to the surface tension and inversely proportional to the viscosity.

Equation 9 can be inverted to calculate an effective viscosity as

$$\eta_{\mathrm{eff}} = \frac{\gamma q}{2R} \tag{10}$$

The viscosity in eq 10 is termed "effective viscosity" because the model makes two assumptions which are not necessarily fulfilled in practice: first, the viscosity may not be homogeneous in space as assumed in eq 6: it may vary with depth, z, if there is surface-induced softening. Our results, in fact, indicate that this is the case. Second, polymers show viscoelastic dispersion: the viscosity is a complex function of frequency. As a consequence, the decay curves are not exponentials but more complicated functions. In ref 15, we have elaborated on the fact that the complete viscoelastic spectrum can be derived from the decay curve. Here we confine ourselves to an evaluation of the *initial* slope (500 min). This part of the decay is governed by the high frequency viscosity, which, in turn, is governed by local interactions (as opposed to the dynamics of entire chains). It is generally assumed that the glass transition is a local phenomenon unrelated to chain entanglement, which justifies the use of the initial slope.

In principle, this analysis holds for a superposition of different surface waves as well. Since eq 7 is linear in u_0, different surface waves decay independently. The decay rate may depend on the q-vector for two reasons. The first one is explicitly captured in the analysis provided above. While the Laplace pressure scales as

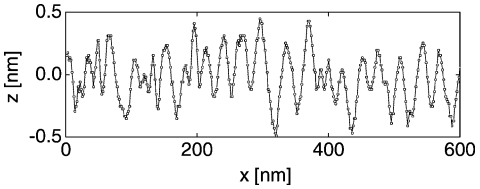

Figure 2. A vertical cut through the surface of the master. The wavelength of the corrugation grating is about 40 nm, and the modulation depth is about 0.8 nm peak-to-peak. Clearly, the grating is not periodic.

q^2, the viscous stress only scales with q (eq 6). Since the speed of the decay results from the competition between surface tension and viscosity, there is a factor of q in the decay rate (eq 9). However, the decay rate may also depend on wavelength because the *penetration depth* of a surface wave is proportional to its wavelength. If the surface-induced softening is limited to a shallow region beneath the surface, only the surface waves with a small penetration depth (that is, a short wavelength) will feel it. Comparing the decay rates for different q-vectors therefore amounts to a depth profiling.

Sample Preparation

The polystyrene samples (M_w = 65 kg/mol, M_w/M_n = 1.02; PSS, Mainz, Germany) were prepared by spin-casting a 90 g/L toluene solution at 400 rpm on a silicon substrate. The substrate had been cleaned by sonication in Hellmanex (HELLMA, Germany), rinsing in Milli-Q water, ultrasonic cleaning and rinsing in ethanol, and drying with N_2. To remove residual solvent, the cast films were vacuum-annealed for 12 h at 100 °C.

The master for the hot-embossing process was formed by ultrahigh-vacuum annealing of a silicon single-crystal surface with its surface normal pointing some 3° off the ⟨113⟩ direction toward the ⟨001⟩ direction. Upon thermal annealing, the surface energy is lowered by the formation of facets of (113) and (114) orientation, respectively. The resulting grooves between the (113) and (114) facets all point along the $(1\bar{1}0)$ direction, leading to a macroscopically large area of uniformly oriented surface corrugation. The lateral size of the terraces perpendicular to the groove direction can be adjusted via the annealing time, the annealing temperature, and the particular protocol used for sample preparation. Once the desired lateral size of the grating is reached, the resulting structure is frozen by cooling the sample to room temperature. Subsequently, the ultrahigh-vacuum chamber is vented and the silicon surface is rapidly covered by a layer of native silicon oxide. However, since the thickness of the native oxide layer amounts to only some 1−2 nm, the corrugation is conserved.[17,18]

To reduce adhesion of the polymer on the master during imprinting, the master was coated with a self-assembled monolayer of fluorosilane ((tridecafluoro-1,1,2,2-tetrahydroctyl)triethoxysilane ($C_{14}H_{19}F_{13}O_3Si$); ABCR, Karlsruhe, Germany). The deposition was carried out from the vapor phase in an argon atmosphere.

Since the angle between neighboring (113) and (114) facets on the corrugated silicon surface is fixed, the vertical amplitude of the grating is proportional to its mean lateral spacing, and the ratio between the peak-to-peak amplitude and the average spacing is about 1/50. The profile in Figure 2 shows an indication of an underlying triangular pattern. Since the terrace formation is a statistic process, the induced surface grating is not periodic. From the structure factor of an AFM micrograph taken of the embossed surface (Figure 4a) one infers a spread $\Delta q/q_{max}$ of about 1, where q_{max} is the wave vector corresponding to the maximum of the structure factor and Δq is the half-band-full-width of the peak.

For hot-embossing both the master and the sample were heated to the embossing temperature of 160 °C. When the embossing temperature had been reached, the master was lowered into the soft polymer melt. After an embossing time of 2 h, the temperature was lowered to room temperature at a rate of 3 °C/min. The master was lifted off at room temperature. The embossing temperature of 160 °C was chosen in order to allow for a fast polymer flow while staying safely away from the decomposition temperature of PS. The embossing time of 2 h was much longer than the terminal relaxation time of the polymer. This procedure ensures that the polymer chains near the surface are relaxed after the imprinting process.

Experimental and Data Analysis

The AFM measurements were performed with a MultiMode scanning probe microscope (NanoScope III controller) equipped with a temperature control unit (Nanoscope MMHTRS) from Digital Instruments. We have independently calibrated the temperature scale with a PT100 sensor placed at the location of the sample. The effect of the laser on the sample temperature was less than 0.5 °C.

We used the TappingMode with cantilevers of 125 μm length (Nanosensors). All images were taken under "light tapping conditions"[21] (amplitude $A_0 \approx 70$ nm; $A_{sp}/A_0 \approx 0.8$, with A_{sp} the set-point amplitude) to minimize the influence of the imaging process onto the sample properties. We checked for tip-induced modifications of the sample by increasing the size of an image after a certain central area had been imaged for an extended period of time at 70 °C. The central area of this enlarged area was in no way different from the rest of the image, which makes us conclude that the imaging process is nondestructive.

An image size of 3.5 μm × 3.5 μm (corresponding to a pixel size of 6.8 nm) was found to be the best compromise between the need to resolve the grating and the need to image large enough areas for statistical analysis. The scanning direction was perpendicular to the grooves. The cantilever was retracted when changing the temperature. Occasionally, the parameters of operation had to be readjusted after a temperature step in order to ensure optimum operation.

For analysis, the one-dimensional structure factor $S(q)$ was computed by fast Fourier transformation (FFT) and accumulated for all lines of an image (full line in Figure 4). The structure factor contains the squares of the moduli of the Fourier components. There is a substantial background, which increases with decreasing q. The background can be independently determined by repeating the analysis for the columns of the image, where the columns run *along* the grooves (dashed lines in Figure 4). Note, however, that the analysis holds for any kind of surface structure: background subtraction is not needed. The analysis presented below is based on the spectra derived from the horizontal lines.

Neither the resolution of the AFM nor its calibration affects the outcome of the analysis much. The derivation

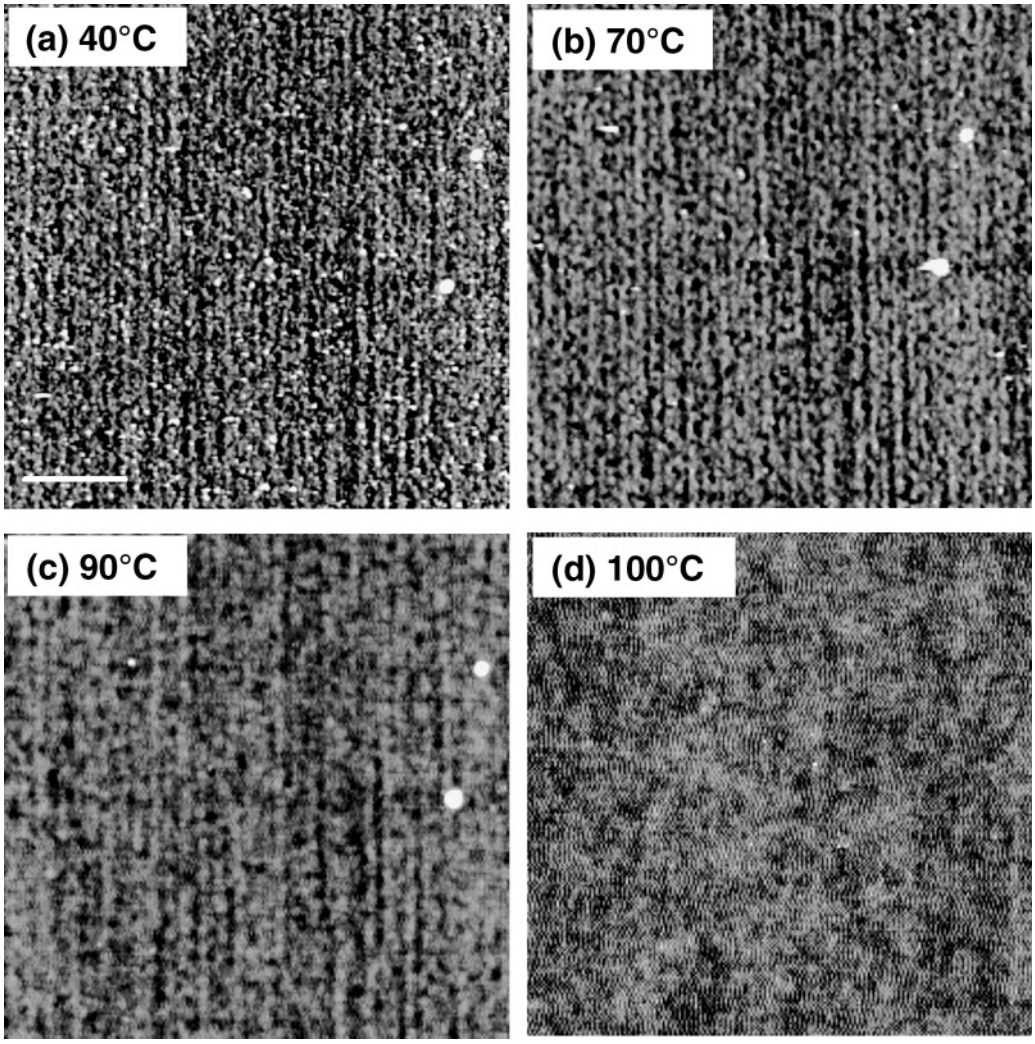

Figure 3. AFM micrographs of an embossed polystyrene surface at 40, 70, 90, and 100 °C. For clarity, only a part of the original image with a size of 1.5 μm × 1.5 μm is shown. The location remained unchanged as indicated by the spots on the right-hand side. The spots have disappeared at 100 °C. The bar corresponds to 300 nm. The gray scale covers a vertical range of 10 nm.

of the effective viscosity is based on the decay rate of the gratings. As long as the gratings are clearly visible (which is the case) quantification of the topographical information is unessential.

Results and Discussion

We report on two sets of experiments. In a first temperature ramp experiment, a freshly prepared grating was heated to its glass temperature in steps of 10 K. At temperatures of 40, 50, 60, 70, 80, 90, and 100 °C the heating process was interrupted for about 30 min while images were taken. Figure 3 shows a selection of AFM images of the temperature ramp. Subsets of 1.5 μm × 1.5 μm size have been enlarged for clarity. Figure 4 shows the structure factor derived from Figure 3a−c. For Figure 3d (T = 100 °C) the feedback loop of the instruments started to oscillate with a period corresponding to about 3 pixels. This artifact prevents a statistical analysis. Visual inspection of the AFM images shows that the grating has disappeared.

In the following we discuss the roughness as a function of temperature. We display data for temperatures larger than 40 °C. Actually, there is a slight increase in the amplitude of roughness when we start the experiment, heating from room temperature to 40 °C. Figure 5 shows partial root-mean-square (rms)

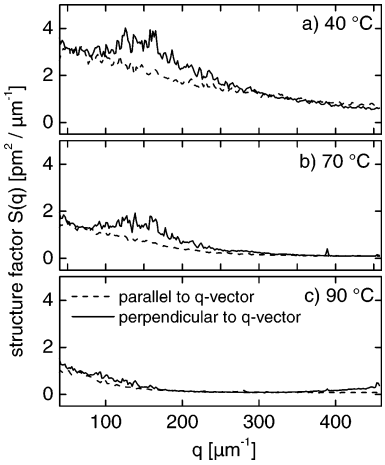

Figure 4. Structure factor of the AFM images of from Figure 2: full, accumulated structure factor of all horizontal lines; dashed, accumulated structure factor of all vertical columns.

roughnesses vs temperature. By a partial rms roughness we mean the square root of the integrated structure factor, where the integration is only carried out over a certain limited q range. If the range of integration is unlimited, the conventional rms roughness results because of the relation $\delta z_{\mathrm{rms}} = (\int |\delta z(q)|^2 \, \mathrm{d}q)^{1/2}$, where

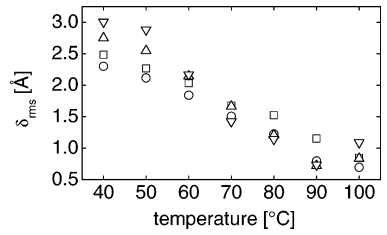

Figure 5. Partial root-mean-square roughness, where the integration has been limited to certain q ranges: (▽) $q = 125-157\ \mu m^{-1}$, $\lambda_{av} = 44$ nm, $\xi_{av} = 7$ nm; (△) $q = 157-209\ \mu m^{-1}$, $\lambda_{av} = 34$ nm, $\xi_{av} = 5.5$ nm; (□) $q = 209-314\ \mu m^{-1}$, $\lambda_{av} = 24$ nm, $\xi_{av} = 3.8$ nm; (○) $q = 314-440\ \mu m^{-1}$, $\lambda_{av} = 16$ nm, $\xi_{av} = 2.6$ nm.

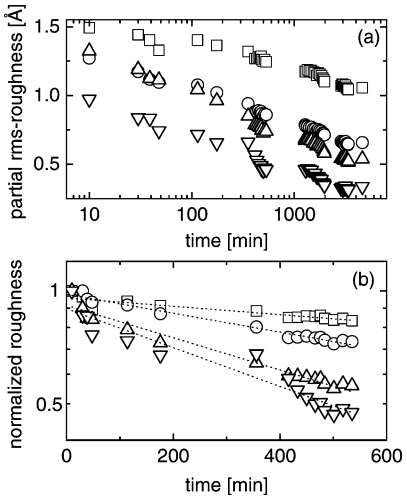

Figure 6. Decay of the partial root-mean-square roughness with time: (□) $q = 125-157\ \mu m^{-1}$, (△) $q = 157-209\ \mu m^{-1}$, (○) $q = 209-314\ \mu m^{-1}$, (▽) $q = 314-440\ \mu m^{-1}$. The temperature of the sample was 70 °C. Panel b shows the initial range, where the roughness was normalized to its value at $t = 0$. The dashed lines are fits to an exponential decay.

$|\delta z(q)|^2$ is the structure factor. Figure 5 shows the partial root-mean-square roughness where the ranges of integration are 125−157, 157−209, 209−314, and 314−440 μm^{-1}. These q ranges correspond to average wavelengths of 44, 34, 24, and 16 nm, respectively. The average penetration depths are 7.1, 5.5, 3.8, and 2.6 nm. At a temperature of 70 °C (which is 30 °C below the bulk T_g), the rms roughness has decayed to about half of its value at 40 °C. The different wavelengths do not decay at the same rate: as expected from eq 9, the high-frequency components decay first. At 90 °C the decay is almost complete, although some structure remains. These data show that the material close to the interface flows much faster than expected. This is a very general statement which does not make use of the theory outlined above.

To make the analysis more quantitative, we have performed a kinetic experiment at a fixed temperature of 70 °C. Figure 6 shows the partial root-mean-square roughness in the same q ranges as in Figure 5. As in the temperature ramp experiments, the high-frequency waves decay faster than the waves with a small frequency (long wavelength). Panel b displays the initial part of the decay ($t \leq 500$ min) in a semilogarithmic plot, where all roughnesses have been normalized to their initial value. Evidently, there is some arbitrariness in the definition of the "initial" slope. Had we confined the analysis to the first 60 min, the decay rates would have been larger and the derived effective viscosities would have been even smaller. The dotted lines in Figure 6b are best fits to exponential decays in the range of 0−500 min. The decay rates are 4.2×10^{-6}, 9.6×10^{-6}, 16.5×10^{-6}, and $19.8 \times 10^{-6}\ s^{-1}$ for the q ranges of 125−157, 157−209, 209−314, and 314−440 μm^{-1}, respectively. Using eq 10 together with a surface tension of polystyrene at $T = 70$ °C of 37 ± 1 mN/m,[22] one derives an effective viscosity of 6.2×10^{11}, 3.6×10^{11}, 3.0×10^{11}, and 3.6×10^{11} Pa s for the different q ranges, respectively (Table 1 and Figure 7). The error bars on the viscosity originate from the uncertainty in the determination of the decay rate from Figure 6b.

Table 1. Parameters and Results of the Kinetic Experiments at $T = 70$ °C

λ [nm]	q [10^6/m]	penetration depth [nm]	decay rate R [10^{-6}/s]	viscosity η^a [10^{11} N/m]
40−50	125−157	6.4−8.0	4.2 ± 0.5	6.2 ± 1
30−40	157−209	4.8−6.4	9.6 ± 1.1	3.6 ± 0.6
20−30	209−314	3.2−4.8	16.5 ± 1.5	3.0 ± 0.8
14−20	314−440	2.3−3.2	19.8 ± 2.7	3.6 ± 0.8

[a] The viscosity is derived from the initial decay rate by eq 10.

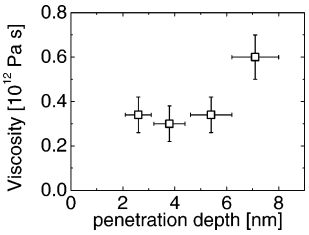

Figure 7. Effective viscosities derived from the initial decay rates (Figure 6) and eq 10 vs penetration depth.

The derived effective viscosities are slightly below 10^{12} Pa s. This is less than the viscosity of the bulk polymer at T_g, where we adopt the definition of the glass temperature, according to which the viscosity is 10^{12} Pa s at T_g. The equivalent temperature (where the bulk material would yield the same decay rate) therefore is slightly above the bulk T_g of 103 °C. Given that the experiment was carried out at 70 °C, the decrease of T_g near the surface amounts to about 30 K. Interestingly, there is a q dependence of the effective viscosity, meaning that the effective viscosity depends on the penetration depth. The shallow (high q) waves probe a region closer to the surface, whereas the low-q waves probe a region that reaches farther into the bulk. There is a slight increase of the viscosity for the largest penetration depth investigated, meaning that the deepest wave already probes the increase of the viscosity with depth.

Our findings are in line with many of the studies on thin films[5] and also with the results obtained with friction force microscopy on polymer surfaces.[1] They are at variance with previous work on the decay of surface roughness[13] and reorientation upon buffing,[10] where there was no or little evidence for a decreased T_g near the surface. As pointed out before, the depression of T_g near the surface depends on details of the experiment. In particular, we cannot rule out an influence of the imprinting procedure. Although the imprinting was carried with long imprinting times at a temperature much above T_g, the memory may not have completely been erased. Note, however, that our experiment mimics the hot embossing process as it is performed in many technical environments. We report a decreased T_g of a polystyrene sample which has undergone a gentle imprinting process. This result applies to many practical

situations because all technical materials have been put into their shapes in one way or another.

Conclusions

Nanoscale corrugation gratings which have been imprinted into a glass-forming polymer surface were found to decay at elevated temperature due to surface tension. The decay is much faster than expected. The near-surface T_g is more than 30 K below the T_g of the bulk. The technique allows for depth profiling. The acceleration of the decay is less pronounced for waves which extend deeper into the bulk. The available spectrum of surface waves covered a range of penetration depths between 2.6 and 7.1 nm. The fact that the effective viscosity depends on the penetration depth indicates that the surface-induced softening is confined to the first few nanometers below the surface.

Acknowledgment. We thank Tadeusz Pakula for providing the rheological data on the bulk polystyrene and Svetlana Gourianova for help with the experiment. Part of this work was funded by the Deutsche Forschungsgemeinschaft in the frame of the Sonderforschungsbereich 262, D13. The corrugated silicon surfaces were developed with the financial support by the Deutsche Forschungsgemeinschaft (Schwerpunktprogramm "Benetzung und Strukturbildung an Grenzflächen" (Kr1269/9).

References and Notes

(1) Kajiyama, T.; Tanaka, K.; Satomi, N.; Takahara, A. *Macromolecules* **1998**, *31*, 5150.
(2) Wang, X. P.; Xiao, X. D.; Tsui, O. K. *Macromolecules* **2001**, *34*, 4180.
(3) Brown, H. R. *Annu. Rev. Mater. Sci.* **1991**, *21*, 463.
(4) Bushan, B., Ed.; *Handbook of Micro/Nano Tribology*; CRC Press: Boca Raton, FL, 1995.
(5) Forrest, J. A.; Jones, R. A. L. *Polym. Surf., Interfaces, Thin Films* **2000**, 251−294.
(6) Forrest, J. A.; Dalnoki-Veress, K.; Stevens, J. R.; Dutcher, J. R. *Phys. Rev. Lett.* **1996**, *77*, 2002.
(7) Sills, S.; Overney, R. M. *Phys. Rev. Lett.* **2003**, *9109*, 5501.
(8) Forrest, J. A.; Svanberg, C.; Revesz, K.; Rodahl, M.; Torell, L. M.; Kasemo, B. *Phys. Rev. E* **1998**, *58*, R1226.
(9) Zaporojtchenko, V.; Strunskus, T.; Erichsen, J.; Faupel, F. *Macromolecules* **2001**, *34*, 1125.
(10) Liu, Y.; Russell, T. P.; Samant, M. G.; Stöhr, J.; Brown, H. R.; Cossy-Favre, A.; Diaz, J. *Macromolecules* **1997**, *30*, 7768.
(11) Seydel, T.; Tolan, M.; Ocko, B. M.; Seeck, O. H.; Weber, R.; DiMasi, E.; Press, W. *Phys. Rev.* B **2002**, *6518*, 4207.
(12) Wang, J.; Tolan, M.; Seeck, O. H.; Sinha, S. K.; Bahr, O.; Rafailovich, M. H.; Sokolov, J. *Phys. Rev. Lett.* **1999**, *83*, 564.
(13) Kerle, T.; Lin, Z. Q.; Kim, H. C.; Russell, T. P. *Macromolecules* **2001**, *34*, 3484.
(14) Li, Z.; Tolan, M.; Hohr, T.; Kharas, D.; Qu, S.; Sokolov, J.; Rafailovich, M. H.; Lorenz, H.; Kotthaus, J. P.; Wang, J.; Sinha, S. K.; Gibaud, A. *Macromolecules* **1998**, *31*, 1915.
(15) Hamdorf, M.; Johannsmann, D. *J. Chem. Phys.* **2000**, *112*, 4262.
(16) Petersen, K.; Johannsmann, D. *J. Non-Cryst. Solids* **2002**, *307*, 532.
(17) Song, S.; Mochrie, S. G. J.; Stephenson, G. P. *Phys. Rev. Lett.* **1995**, *74*, 5240.
(18) Rehse, N.; Wang, C.; Hund, M.; Geoghegan, M.; Magerle, R.; Krausch, G. *Eur. Phys.* E **2001**, *4*, 69.
(19) Levich, V. G. *Physicochemical Hydrodynamics*; Prentice-Hall: Englewood Cliffs, NJ, 1962.
(20) Harden, J. L.; Pleiner, H.; Pincus, P. A. *J. Chem. Phys.* **1991**, *94*, 5208.
(21) Magonov, S. N.; Elings, V.; Whangbo, M. H. *Surf. Sci. Lett.* **1997**, *375*, L385.
(22) Dee, G. T.; Sauer, B. B. *J. Colloid Interface Sci.* **1992**, *152*, 85.

MA049595Z